Dalton Transactions

ROYAL SOCIETY OF CHEMISTRY

PAPER

View Article Online
View Journal | View Issue

Check for updates

Cite this: *Dalton Trans.*, 2023, **52**, 4475

The structure and modified properties of a self-dimerised Cu(II) inclusion complex in γ-cyclodextrins†

Tomohiko Hamaguchi, *[a] Ryuta Ishikawa, [a] Akio Mishima,[b] Shinya Hayami, [c,d] Masaaki Ohba, [b] Minoru Satoh[e] and Satoshi Kawata [a]

Received 19th January 2023,
Accepted 1st March 2023

DOI: 10.1039/d3dt00176h

rsc.li/dalton

Inclusion structures incorporating more than one guest molecule are elusive because confinement alters their molecular properties. We report the solid-state characterization of an inclusion complex comprising two γ-cyclodextrins and two [Cu(2-pyridinemethanolate)(2-pyridinemethanol)]PF_6 units. Quantum calculation reveals that *interfragment charge transfer* occurs. The confined Cu fragment and the unincluded "linear chain [Cu(2-pyridinemethanolate)(2-pyridinemethanol)]PF_6" exhibit different properties.

Introduction

Molecular confinement is an attractive method not only to modulate molecular features, such as light absorption and emission, and electrochemical properties,[1] but also to regulate unique chemical reactions by altering the chemical reactivity of the confined molecules.[2] For instance, controlled polymers can be synthesized from aligned monomers through confinement.[3]

To this end, cyclodextrins (CDs), which are cyclic oligosaccharides consisting of D-glucose subunits,[4] are widely used because their hydrophobic cavities can accommodate organic compounds, polyoxometalates, metal clusters and coordination complexes,[5,6] whose redox, spin, and luminescence properties are modified as a result of their confinement.[7–9] In fact, a search in the CCDC database (updated in June 2022) resulted in more than 350 articles reporting the crystal structure of inclusion complexes of CDs. In contrast, reports on CD inclusion complexes with more than one guest molecule are scarce.[10,11]

We previously examined the inclusion equilibrium of a bis(2-pyridinemethanolate) Cu(II) complex and CDs in solution,[12] finding that the Cu complex dimerises when confined in γ-CD; however, all experiments were conducted in solution, and no data were obtained in the solid state. Herein, we describe the isolation of single crystals of the inclusion complex $\{[Cu(L)(HL)]_2@(\gamma\text{-CD})_2\}(PF_6)_2$ (**1**) (L = 2-pyridinemethanolate, HL = 2-pyridinemethanol) and their solid-state characterization *via* X-ray diffraction, spectroscopy, and magnetic studies. On the basis of the results, we discuss the effect of the confinement in the cavity of γ-CD on the structure and properties of the Cu complex.

Results and discussion

Effect of confinement in the cavity of γ-CD on the structure of the Cu complex

The crystal structure of the inclusion complex **1** is shown in Fig. 1, S1, and S2.† The complex crystallizes in the chiral space group $P2_12_12$. The crystal contains two $[Cu(L)(HL)]^+$ cations, two PF_6^- counter anions, two γ-CDs and 35 water of crystallization molecules. Two γ-CDs form one host *via* the interaction of their secondary rims[13,14] by direct hydrogen bonding and through interaction with solvent water molecules (Fig. S3†), with a dimeric assembly of two parallel planar $[Cu(L)(HL)]^+$ fragments included in the cavity. Only the pyridyl moieties are held in γ-CD, and the Cu centers are located in a gap between the secondary rims. Some solvent water molecules included in the gap help stabilize the dimeric $[Cu(L)(HL)]^+$ assembly in the cavity *via* hydrogen bonding. Other water molecules surround

[a]*Department of Chemistry, Faculty of Science, Fukuoka University, 8-19-1 Nanakuma, Jonan-ku, Fukuoka 814-0180, Japan. E-mail: thama@fukuoka-u.ac.jp*
[b]*Department of Chemistry, Faculty of Sciences, Kyushu University, 744 Motooka, Nishi-ku, 819-0395 Fukuoka, Japan*
[c]*Department of Chemistry, Graduate School of Science and Technology, Kumamoto University, 2-39-1, Kurokami, Chuo-ku, Kumamoto 860-8555, Japan*
[d]*Institute of Pulsed Power Science, Kumamoto University, 2-39-1, Kurokami, Chuo-ku, Kumamoto 860-8555, Japan*
[e]*Department of Industrial Engineering, National Institute of Technology (KOSEN), Ibaraki College, 866 Nakane, Hitachinaka-shi, Ibaraki-ken 312-8508, Japan*

†Electronic supplementary information (ESI) available: Crystal structure, titration, computational study data, circular dichroism, PXRD data, the residual density map, and a movie of the crystal structure. CCDC 2220549. For ESI and crystallographic data in CIF or other electronic format see DOI: **https://doi.org/10.1039/d3dt00176h**

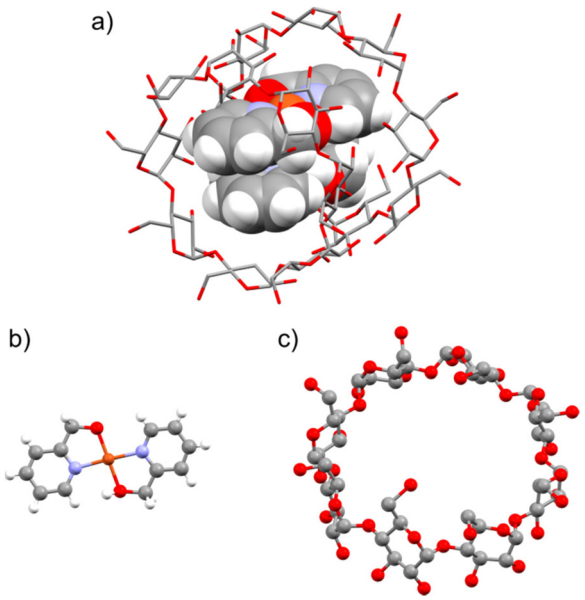

Fig. 1 Molecular structures of (a) the inclusion complex **1**·35H_2O shown by CPK model ($[Cu(L)(HL)]^+$) and capped stick model (γ-CD), (b) $[Cu(L)(HL)]^+$ shown by ball-and-stick model, and (c) γ-CD shown by ball-and-stick model. Orange: Cu, red: O, grey: C, blue: N, white: H. Counter anions, water molecules, and protons except for $[Cu(L)(HL)]^+$ are omitted for clarity.

the γ-CDs. No water molecules are included in the γ-CD cavity. The included complex is arranged in a tubular shape by interconnecting through the primary rims[15,16] *via* direct hydrogen bonding and through solvent water molecules (Fig. S4†). The gap between primary rims is occupied by counter anions. The dimeric $[Cu(L)(HL)]^+$ assembly shows π–π stacking between the pyridine rings (distances between the pyridyl ring centroids = 3.665(5), 3.642(6) Å; Fig. S5†). Two solvent water molecules connect two $[Cu(L)(HL)]^+$ fragments by hydrogen bonding (the $O_{HL}\cdots O_{water}$ and $O_L\cdots O_{water}$ distances are 2.68(1) and 2.78(1) Å, respectively), whereas no direct hydrogen bonding is formed between L and HL ($O_L\cdots O_{HL}$ = 4.09(1) Å). The distance between two Cu atoms is 3.755(2) Å, which means that there is little metal–metal bond character. The τ_4 value (0.07) and the dihedral angle of the two Cu–O–N planes (6.5(3)°) indicate that the $[Cu(L)(HL)]^+$ fragment shows a slightly distorted square-planar geometry.

The $[Cu(L)(HL)]^+$ fragment without γ-CD and its deprotonated complex have been previously isolated as $[Cu(L)(HL)]PF_6$ (**2**)[17] and $[Cu(L)_2]\cdot 4H_2O$ (**3**),[18] respectively. Although complexes **2** and **3** are synthesized under different pH conditions (pH ∼ 4 and 10, respectively), they can be interconverted *via* recrystallization.[17] The corresponding X-ray crystallographic study revealed that complexes **2** and **3** show a completely square-planar geometry. Complex **2** has a linear chain structure connected by relatively strong direct hydrogen bonds between L and HL, whereas complex **3** exhibits a 2D network structure connected by hydrogen bonding with solvent water molecules. By comparing the structures of inclusion complex **1** and complex **2**, it can be considered that in inclusion complex **1**, two γ-CDs extract two $[Cu(L)(HL)]^+$ fragments from the linear chain structure to include them into the cavity. It is also interesting that the same fragments in **1** and **2** show different stacking. A Cu ion of the inclusion complex **1** is placed at the apical position of the other; however, a Cu ion of the linear chain complex **2** is located over the pyridyl ring of the other. This difference can be attributed to the confinement. As mentioned before, the $[Cu(L)(HL)]^+$ fragment in the cavity has a slightly distorted square-planar structure, whereas that of complex **2** is completely square planar. The distortion is caused by the confinement in the chiral γ-CD. As a result, the dimeric assembly shows chirality, as was revealed by circular dichroism measurements (see below).

We previously described that the inclusion complex is formed from $[Cu(L)_2]$ and CDs.[12] Although we synthesized $[Cu(L)_2]$ *via* recrystallization from water at pH ∼ 9, we measured the electron spin resonance (ESR) spectra and the absorption/circular dichroism spectra of the complex with CDs under moderately acidic conditions (pH = 6.5 and 7.15, respectively). In the present study, we performed a rough titration, and the result revealed that the protonated complex appeared at around pH ∼ 7 (Fig. S6 and Table S1†). This suggests that the Cu fragment in CDs was $[Cu(L)(HL)]^+$ instead of $[Cu(L)_2]$. Moreover, according to the ESR and circular dichroism results, we previously speculated that the Cu fragment formed a 2 : 1 inclusion complex with γ-CD. However, the $[Cu(L)(HL)]^+$ fragment forms a parallel planar dimeric assembly upon confinement in two γ-CDs, resulting in a 2 : 2 complex. The hypothesis about the structure of the dimerised Cu complex is in accordance with the result of the single-crystal X-ray analysis, in particular, with the interplanar distance of the $[Cu(L)(HL)]^+$ fragments and the distance between the two Cu atoms.

To confirm that the inclusion complex was $[Cu(L)(HL)]^+$ and not $[Cu(L)_2]$, we conducted quantum calculations in solution, finding that the formation of the dimeric assembly from two Cu fragments occurs preferentially for $[Cu(L)(HL)]^+$ over $[Cu(L)_2]$ (Tables S2–S12†). In addition, the stacked structure of $[Cu(L)(HL)]^+$ is different from that of $[Cu(L)_2]$ (Fig. S7†). Specifically, two $[Cu(L)(HL)]^+$ fragments are completely overlaid on each other due to the formation of hydrogen bonding (O–H···O) and π–π stacking between the pyridyl rings; however, two $[Cu(L)_2]$ fragments form an incomplete stacking owing to Cu···O interactions, which does not fit the cavity of γ-CD.

Effect of confinement in the cavity of γ-CD on the properties of the Cu complex

Circular dichroism. We investigated the induced circular dichroism.[19,20] Fig. 2 shows the circular dichroism and absorption spectra of the inclusion complex measured in the solid state. The inclusion complex produces a broad absorption band between 400 and 800 nm, and a circular dichroism band appears at around the same region. The absorption band is also observed for complex **2**, which does not exhibit a circular dichroism band (Fig. S8†). This behavior, which is similar to

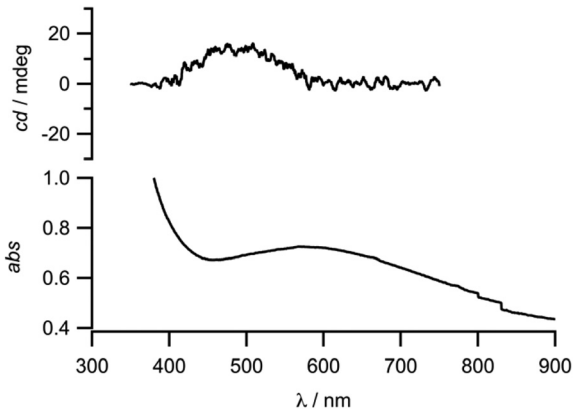

Fig. 2 Circular dichroism (top) and absorption (bottom) spectra of the inclusion complex **1**·31H_2O.

that observed in solution,[12] demonstrates that the $[Cu(L)(HL)]^+$ fragment has chirality induced by γ-CD.

ESR. As shown in the X-ray crystal structure, two Cu fragments are tightly packed in the cavity of γ-CD. This interaction can be expected to affect the properties of the Cu fragment, which would behave differently in dimeric and monomeric forms. To estimate the interaction between the Cu fragments, we performed ESR and magnetic susceptibility measurements. Fig. 3 shows the ESR spectrum of the powder of the inclusion complex **1** at room temperature. The signal at around 0.33 T can be attributed to the $\Delta M_s = \pm 1$ transition of two Cu(II) ions ($S = 1$), and hyperfine splitting was clearly observed. Another signal around at 0.16 T is ascribable to the $\Delta M_s = \pm 2$ transition. This behavior is similar to that observed in the solution state, as previously reported.[12] The spectrum implies that the dimeric assembly is isolated from others even in the solid state, which is supported by the shortest interdimeric assembly Cu···Cu distance of 14.8 Å found in the X-ray crystal structure (Fig. S9†). A similar behavior has been reported in the discrete stacking of a mononuclear Cu(II) complex within an organic-pillared coordination cage;[21] however, in our case, γ-CD can isolate a dimeric assembly completely.

Magnetic behavior. The isolation of the dinuclear complex was further confirmed by the magnetic susceptibility data (Fig. 4). The magnetic behavior can be attributed to a magnetically isolated Cu(II) dinuclear complex. The $\chi_{mol}T$ *vs.* T plot was simulated by assuming that the inclusion complex was a Cu(II) dinuclear complex. A spin Hamiltonian (eqn (1)) and eqn (2) were used in the curve fitting:

$$H = -2JS_1S_2 \quad (1)$$

$$\chi_{mol}T = \frac{Ng^2\beta^2}{k}\left[\frac{1}{3 + (\exp(-J/kT))^2}\right] \times 2 \quad (2)$$

The best-fit parameters were $g = 2.02$ and $J = -0.83(1)$ cm^{-1}. The J value means that the antiferromagnetic exchange coupling between Cu atoms is weaker than that of the linear chain complex **2**. The different stacking is most likely responsible for the difference in the magnetic behavior.

Calculated absorption spectrum. The interaction was also confirmed by the absorption spectrum obtained *via* quantum calculation. The simulated absorption spectra of the monomeric $[Cu(L)(HL)]^+$ fragment and the dimeric assembly were very similar (Fig. S10†). In the spectrum of the dimeric assembly, 46 transitions can be observed between 300 and 800 nm. There are two transitions attributable to the HOMO−1(beta), the HOMO(beta), the LUMO(beta), and the LUMO+1(beta) at 416 nm. The two $[Cu(L)(HL)]^+$ fragments contribute to the HOMOs almost equally, whereas their contributions to the LUMOs differ (7 : 3 or 3 : 7) (Tables S11, S12 and Fig. S11†). Therefore, these two transitions can be attributed to *interfragment charge transfer*, that is, to the interaction between Cu fragments. It is noteworthy that 30 transitions are classified into this type. Two transitions are classified as *intrafragment charge transfer* and others are unspecified. Unfortunately, the lack of a spectrum of discrete $[Cu(L)(HL)]^+$ fragments prevented us from comparing the observed spectra of the monomeric and dimeric fragments.

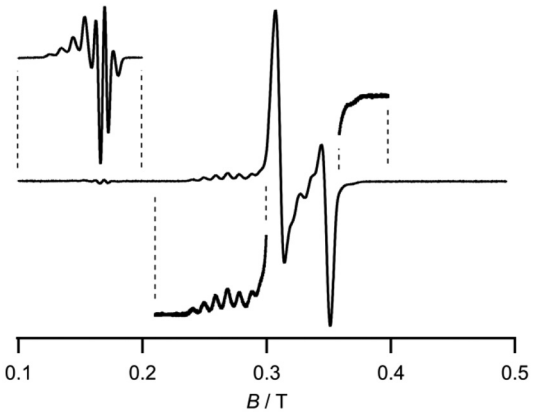

Fig. 3 X-band ESR spectrum of the inclusion complex **1**·31H_2O at room temperature. The microwave frequency was 9.43 GHz.

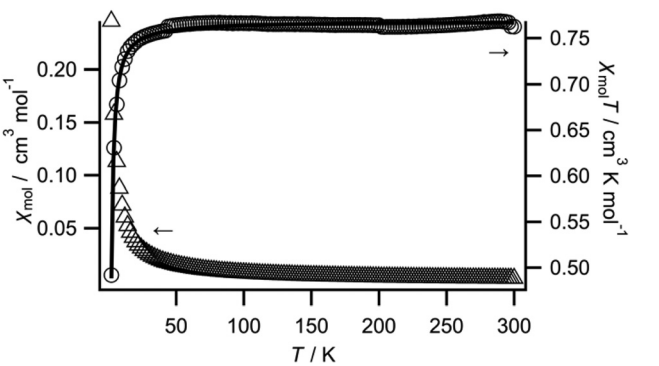

Fig. 4 Plots of $\chi_{mol}T$ *vs.* T and χ_{mol} *vs.* T for the complex **1**·31H_2O (circles: $\chi_{mol}T$; triangles: χ_{mol}). The solid line represents the fit to the data.

Conclusions

In summary, we investigated the inclusion of $[Cu(L)(HL)]^+$ in the cavity of γ-CD in the solid state. Two $[Cu(L)(HL)]^+$ fragments form one dimeric assembly, which is included in the cavity formed by two γ-CDs interconnected through their secondary rims. The dimeric assembly shows circular dichroism induced by its tight packing in the chiral cavity of γ-CD. The effect of the tight packing was confirmed by spectroscopic and magnetic studies. The confinement isolates the dimeric assembly. The inclusion behavior of $[Cu(L)(HL)]^+$ in γ-CD was previously reported only in solution, and the resulting structure was speculated to have a Cu fragment:γ-CD ratio = 2 : 1 according to the ESR and circular dichroism spectra. However, the single-crystal X-ray diffraction study presented herein revealed that the inclusion complex is formed by two Cu fragments and two γ-CD units. Furthermore, the included Cu fragment is not $[Cu(L)_2]$ but $[Cu(L)(HL)]^+$, which was supported by a quantum calculation study.

It is interesting that the inclusion complex shows different properties from those of the free complex due not only to the isolation but also to the confinement. Further studies of the inclusion complex are underway in our laboratory.

Experimental section

General methods

All materials were purchased from commercial suppliers (Wako Pure Chemical Industries, Ltd, Kanto Chemical Co., Inc. and Tokyo Chemical Industry Co., Ltd) and used without further purification.

Bulk samples were used for all measurements except for the single-crystal X-ray study, for which air-dried single crystals were used. The single-crystal study revealed that the inclusion complex contained 35 water molecules. Meanwhile, a water content of 31 molecules was determined by elemental analysis for the bulk samples. The powder X-ray diffraction (PXRD) study revealed that the bulk sample showed almost the same structure as that of the single-crystal study (Fig. S12†).

The PXRD data were recorded on a Rigaku MultiFlex X-ray diffractometer using Cu Kα radiation at a wavelength of 1.542 Å. The X-band ESR spectra were acquired with a JEOL RE-1X spectrometer equipped with ES-IPRITS data system software on a personal computer at room temperature. The absorption and circular dichroism spectra were measured on a SIMADZU UV-3600 UV–vis–NIR spectrophotometer and a Jasco J-820 circular dichroism spectrometer, respectively, using KBr pellets. The pH was measured using a DKK-TOA HM-40S pH meter with a two-point calibration (pH 4.01 and 6.89). C, H and N analysis was conducted by the Service Center of the Elementary Analysis of Organic Compounds of Kyushu University.

Synthesis

$[Cu(L)(HL)]PF_6$ was prepared according to a previously reported method.[17]

$\{[Cu(L)(HL)]_2@(\gamma\text{-CD})_2\}(PF_6)_2$ (1). To a solution of $[Cu(L)(HL)]PF_6$ (1.557 g, 3.657 mmol) in CH_3CN (150 mL) was added successively a solution of NH_4PF_6 (0.607 g, 3.724 mmol) in H_2O (10 mL), a solution of γ-CD (4.773 g, 3.680 mmol) in H_2O (50 mL) and a buffer solution (225 mL of 0.1 mol dm^{-3} $NaHCO_3$ aqueous solution and 10.5 mL of 0.1 mol dm^{-3} Na_2CO_3 aqueous solution). The resulting clear blue–purple solution was concentrated by slow evaporation for five days. Finally, the mixture was concentrated to *ca.* 30 mL using a rotary evaporator. The resulting precipitate was filtered and dried under air overnight. **1**·31H_2O (5.186 g, 70.83%). Elemental analysis (%) found: C, 35.7; H, 5.8; N, 1.5. Calc. for $C_{120}H_{186}Cu_2F_{12}N_4O_{84}P_2$·31$H_2O$: C, 36.0; H, 6.2; N, 1.4.

X-ray crystallography

Single crystals of **1** suitable for single-crystal X-ray analysis were obtained by slow recrystallisation from a buffer solution/CH_3CN solution of complex **1** at room temperature, and were mounted in liquid paraffin and transferred to the cold gas stream of the diffractometer. The data were collected on a Rigaku Saturn 724 CCD area-detector diffractometer. A multi-scan absorption correction was applied to the intensity data. The structure was solved by direct methods (SHELXT-2018/2)[22] and then refined by the full-matrix least-squares method on F^2 (SHELXL-2018/3)[23] using the Yadokari-XG (Rev. 1078) software package.[24] All non-hydrogen atoms were refined with anisotropic parameters. The H atoms of water were not included in the final refinement. The H atom of OH in 2-pyCH_2OH was located in a difference Fourier map and the coordinate was fixed. Other H atoms were included in the calculated positions and refined using a riding model. Fig. S13† is the residual density map obtained with the Olex2 (Ver. 1.5) program.[25] Residuals could be assigned to the O atom (oxygen of water) or the H atom (hydrogen of water); however, the PLATON (Ver. 90622) program[26] indicates that there are four solvent accessible areas and that each volume is *ca.* 10 $Å^3$. Crystallographic diagrams were created with the Mercury (Ver. 2022.1.0) program.[27]

Crystal data for **1**·35H_2O: $C_{120}H_{256}Cu_2F_{12}N_4O_{119}P_2$, M = 4076.29 g mol^{-3}, T = 100(2) K, orthorhombic, $P2_12_12$, a = 18.1464(4) Å, b = 28.9479(7) Å, c = 16.4270(4) Å, V = 8629.1(4) $Å^3$, Z = 2, D_{calc} = 1.569 g cm^{-3}, μ = 0.401 mm^{-1}, crystal size 0.42 × 0.10 × 0.08 mm^3, reflections collected 120 168, independent reflections 15 319, R_{int} = 0.0353, goodness-of-fit on F^2 = 1.044, R_1 = 0.0798, wR_2 = 0.2211 (for $I > 2\sigma(I)$), R_1 = 0.0895, wR_2 = 0.2340 (for all data) ($R_1 = \sum||F_o| - |F_c||/\sum|F_o|$. w$R_2 = [\sum w(F_o^2 - F_c^2)^2/\sum w(F_o^2)^2]^{1/2}$), absolute structure parameter = 0.031(3). CCDC 2220549.†

Magnetism

Magnetic susceptibility was measured using a Quantum Design MPMS-5S magnetic property measurement system. Diamagnetic correction (-2.3×10^{-3} cm^3 mol^{-1}), which was calculated using Pascal's constants, was applied.

Computational details

The Gaussian 09 (Rev. D.01) program package[28] was employed for all calculations. To estimate the formation energy of the dimeric $[Cu(L)(HL)]^+$ assembly and the dimeric $[Cu(L)_2]$ assembly, density functional theory (DFT) calculation was performed. The M06L and ωB97XD functionals were used, and the basis sets SDD and 6-31G* were selected for Cu and other atoms, respectively. The initial geometry for geometry optimisation was the modified X-ray structure of $[Cu(L)(HL)]PF_6$ at 100 K.[17] Structural optimisation was conducted in two steps. First, optimisation was performed using the modelled structure without considering the solvent effect. The as-optimised structure was then used as an initial structure for the second optimisation. The solvent effect of water was applied with the default Gaussian PCM implementation. The Facio (Ver. 23.1.5) program[29] was used for molecular modelling. The Facio program and the Gabedit (Ver. 2.5.1) program[30] were used for visualisation of the optimised structures.

To simulate the absorption spectrum, TD-DFT computation was conducted to calculate the excited states in the gas phase at the single point of the dimeric $[Cu(L)(HL)]^+$ assembly and the monomeric $[Cu(L)(HL)]^+$ fragment obtained from the X-ray crystallography study of **1**. The B3LYP functional was used for the calculation. The basis set was the same as above. The Gabedit program was used for visualisation of the molecular orbitals and the GaussSum (Ver. 3.0) program[31] was used for analysis of the simulated spectrum.

Conflicts of interest

There are no conflicts to declare.

Acknowledgements

This work was partially supported by JSPS KAKENHI (Grant No. 20K05546) and funding from Fukuoka University (Grant No. 205002). The authors thank Dr Yuji Yamada for kind discussion about the quantum calculation.

References

1 A. B. Grommet, M. Feller and R. Klajn, *Nat. Nanotechnol.*, 2020, **15**, 256–271.
2 Y. Inokuma, M. Kawano and M. Fujita, *Nat. Chem.*, 2011, **3**, 349–358.
3 A. Nishijima, Y. Kametani and T. Uemura, *Coord. Chem. Rev.*, 2022, **466**, 214601–214620.
4 G. Crini, *Chem. Rev.*, 2014, **114**, 10940–10975.
5 K. A. Connors, *Chem. Rev.*, 1997, **97**, 1325–1358.
6 D. Prochowicz, A. Kornowicz and J. Lewinski, *Chem. Rev.*, 2017, **117**, 13461–13501.
7 E. Coutouli-Argyropoulou, A. Kelaidopoulou, C. Sideris and G. Kokkinidis, *J. Electroanal. Chem.*, 1999, **477**, 130–139.
8 Y. Chen, H.-L. Chen, Q.-C. Yang, X.-Y. Song, C.-Y. Duan and T. C. W. Mak, *J. Chem. Soc., Dalton Trans.*, 1999, 629–634.
9 Q. Wang, Q. Zhang, Q. W. Zhang, X. Li, C. X. Zhao, T. Y. Xu, D. H. Qu and H. Tian, *Nat. Commun.*, 2020, **11**, 158.
10 S. D. Chatziefthimiou, K. Yannakopoulou and I. M. Mavridis, *CrystEngComm*, 2007, **9**, 976–979.
11 D. Shen, J. A. Cooper, P. Li, Q. H. Guo, K. Cai, X. Wang, H. Wu, H. Chen, L. Zhang, Y. Jiao, Y. Qiu, C. L. Stern, Z. Liu, A. C. Sue, Y. W. Yang, F. M. Alsubaie, O. K. Farha and J. F. Stoddart, *J. Am. Chem. Soc.*, 2020, **142**, 2042–2050.
12 H. Yokoi, M. Satoh and M. Iwaizumi, *J. Am. Chem. Soc.*, 1991, **113**, 1530–1533.
13 A. A. Ivanov, C. Falaise, D. Landy, M. Haouas, Y. V. Mironov, M. A. Shestopalov and E. Cadot, *Chem. Commun.*, 2019, **55**, 9951–9954.
14 A. A. Ivanov, C. Falaise, P. A. Abramov, M. A. Shestopalov, K. Kirakci, K. Lang, M. A. Moussawi, M. N. Sokolov, N. G. Naumov, S. Floquet, D. Landy, M. Haouas, K. A. Brylev, Y. V. Mironov, Y. Molard, S. Cordier and E. Cadot, *Chem. – Eur. J.*, 2018, **24**, 13467–13478.
15 A. A. Ivanov, T. N. Pozmogova, A. O. Solovieva, T. S. Frolova, O. I. Sinitsyna, O. V. Lundovskaya, A. R. Tsygankova, M. Haouas, D. Landy, E. Benassi, L. V. Shestopalova, C. Falaise, E. Cadot, M. A. Shestopalov, P. A. Abramov and M. N. Sokolov, *Chem. – Eur. J.*, 2020, **26**, 7479–7485.
16 C. Falaise, A. A. Ivanov, Y. Molard, M. Amela Cortes, M. A. Shestopalov, M. Haouas, E. Cadot and S. Cordier, *Mater. Horiz.*, 2020, **7**, 2399–2406.
17 T. Hamaguchi, T. Nagata, S. Hayami, S. Kawata and I. Ando, *Dalton Trans.*, 2017, **46**, 6196–6201.
18 B. Antonioli, D. J. Bray, J. K. Clegg, K. A. Jolliffe, K. Gloe, K. Gloe and L. F. Lindoy, *Polyhedron*, 2007, **26**, 673–678.
19 A. Harada, Y. Hu, S. Yamamoto and S. Takahashi, *J. Chem. Soc., Dalton Trans.*, 1988, 729–732.
20 X. Cheng, Z. Lu, Y. Li, Q. Wang, C. Lu and Q. Meng, *Dalton Trans.*, 2011, **40**, 11788–11794.
21 M. Yoshizawa, K. Ono, K. Kumazawa, T. Kato and M. Fujita, *J. Am. Chem. Soc.*, 2005, **127**, 10800–10801.
22 G. Sheldrick, *Acta Crystallogr., Sect. A: Found. Adv.*, 2015, **71**, 3–8.
23 G. Sheldrick, *Acta Crystallogr., Sect. C: Struct. Chem.*, 2015, **71**, 3–8.
24 C. Kabuto, S. Akine, T. Nemoto and E. Kwon, *J. Crystallogr. Soc. Jpn.*, 2009, **51**, 218–224.
25 O. V. Dolomanov, L. J. Bourhis, R. J. Gildea, J. A. K. Howard and H. Puschmann, *J. Appl. Crystallogr.*, 2009, **42**, 339–341.
26 A. L. Spek, *J. Appl. Crystallogr.*, 2003, **36**, 7–13.
27 C. F. Macrae, I. Sovago, S. J. Cottrell, P. T. A. Galek, P. McCabe, E. Pidcock, M. Platings, G. P. Shields, J. S. Stevens, M. Towler and P. A. Wood, *J. Appl. Crystallogr.*, 2020, **53**, 226–235.
28 M. J. Frisch, G. W. Trucks, H. B. Schlegel, G. E. Scuseria, M. A. Robb, J. R. Cheeseman, G. Scalmani, V. Barone, B. Mennucci, G. A. Petersson, H. Nakatsuji, M. Caricato, X. Li, H. P. Hratchian, A. F. Izmaylov, J. Bloino, G. Zheng, J. L. Sonnenberg, M. Hada, M. Ehara, K. Toyota, R. Fukuda,

J. Hasegawa, M. Ishida, T. Nakajima, Y. Honda, O. Kitao, H. Nakai, T. Vreven, J. A. Montgomery Jr., J. E. Peralta, F. Ogliaro, M. Bearpark, J. J. Heyd, E. Brothers, K. N. Kudin, V. N. Staroverov, T. Keith, R. Kobayashi, J. Normand, K. Raghavachari, A. Rendell, J. C. Burant, S. S. Iyengar, J. Tomasi, M. Cossi, N. Rega, J. M. Millam, M. Klene, J. E. Knox, J. B. Cross, V. Bakken, C. Adamo, J. Jaramillo, R. Gomperts, R. E. Stratmann, O. Yazyev, A. J. Austin, R. Cammi, C. Pomelli, J. W. Ochterski, R. L. Martin, K. Morokuma, V. G. Zakrzewski, G. A. Voth, P. Salvador, J. J. Dannenberg, S. Dapprich, A. D. Daniels, O. Farkas, J. B. Foresman, J. V. Ortiz, J. Cioslowski and D. J. Fox, *Gaussian 09, Revision D.01*, Gaussian, Inc., Wallingford CT, 2013.

29 M. Suenaga, *J. Comput. Chem., Jpn.*, 2005, **4**, 25–32.

30 A. R. Allouche, *J. Comput. Chem.*, 2011, **32**, 174–182.

31 N. M. O'boyle, A. L. Tenderholt and K. M. Langner, *J. Comput. Chem.*, 2008, **29**, 839–845.